6670 *Biochemistry* **2010,** *49,* 6670–6679
DOI: 10.1021/bi100858k

BIOCHEMISTRY
including biophysical chemistry & molecular biology
Article

Structural Analysis of Alternative Complex III in the Photosynthetic Electron Transfer Chain of *Chloroflexus aurantiacus*[†]

Xinliu Gao,[‡] Yueyong Xin,[‡,§] Patrick D. Bell,[‡] Jianzhong Wen,[‡] and Robert E. Blankenship*[,‡]

[‡]*Departments of Biology and Chemistry, Washington University in St. Louis, St. Louis, Missouri 63130, and* [§]*College of Life and Environmental Sciences, HangZhou Normal University, HangZhou, 310036 P. R. China*

Received May 27, 2010; Revised Manuscript Received July 6, 2010

ABSTRACT: The green photosynthetic bacterium *Chloroflexus aurantiacus*, which belongs to the phylum of filamentous anoxygenic phototrophs, does not contain a cytochrome *bc* or *bf* type complex which is found in all other known groups of phototrophs. This suggests that a functional replacement exists to link the reaction center photochemistry to cyclic electron transfer as well as respiration. Earlier work identified a potential substitute of the cytochrome *bc* complex, now named alternative complex III (ACIII), which has been purified from *C. aurantiacus*, identified, and characterized. ACIII functions as a menaquinol:auracyanin oxidoreductase in the photosynthetic electron transfer chain, and a related but distinct complex functions in respiratory electron flow to a terminal oxidase. In this work, we focus on elucidating the structure of photosynthetic ACIII. We found that ACIII is an integral membrane protein complex of ~300 kDa that consists of eight subunits of seven different types. Among them, there are four metalloprotein subunits, including a 113 kDa iron−sulfur cluster-containing polypeptide, a 25 kDa penta-heme *c*-containing subunit, and two 20 kDa monoheme *c*-containing subunits in the form of a homodimer. A variety of analytical techniques were employed in determining the ACIII substructure, including HPLC combined with ESI-MS, metal analysis, potentiometric titration, and intensity analysis of heme staining SDS−PAGE. A preliminary structural model of ACIII is proposed on the basis of the analytical data and chemical cross-linking in tandem with mass analysis using MALDI-TOF, as well as transmembrane and transit peptide analysis.

Bacterial electron transport pathways largely fall into two major categories: the light-driven photosynthetic electron transfer chain and the aerobic or anaerobic respiratory electron transfer chain. Despite the vast differences between photophosphorylation and oxidative phosphorylation, they both couple the chemical reactions between electron donors and electron acceptors to the translocation of protons across the membrane, which then drives ATP formation and other energy-dependent processes (*1*). As a result, the common feature of all electron transport chains is the presence of a proton pump to create the transmembrane proton gradient. In respiratory electron transfer pathways, there may be as many as three types of proton pumping protein complexes reminiscent of mitochondria, depending on environmental factors (*2*). In contrast, the proton pump in all the photosynthetic electron transfer chains was until recently believed to involve a cytochrome bc_1 or b_6f complex, which resembles mitochondrial complex III in terms of overall structure and mechanism (*3*).

In the species tree of bacteria based on 16S rRNA analysis (*4*), the phylum of filamentous anoxygenic phototrophs (FAPs) is not closely related to the other phyla that contain organisms that carry out chlorophyll-based photosynthesis: purple bacteria, cyanobacteria, heliobacteria, green sulfur bacteria, and chloroacidobacteria. Instead, it exhibits a much deeper branching position to the other five bacterial phyla that contain phototrophic representatives (*5*, *6*). Because of this distinctive feature, the study of FAPs may shed an interesting light on the evolutionary development of photosynthesis. The FAPs make up a very diverse and unique phylum of bacteria, including several genera: *Chloroflexus* (*7*), *Oscillochloris* (*8*), *Chloronema* (*9*), *Heliothrix* (*10*), and several *Chloroflexus*-like bacteria found in marine environments (*11*). Among them, *Chloroflexus aurantiacus*, a prominent microorganism of hot spring microbial mat communities, was the first described and is the most extensively studied representative of FAPs in terms of its photosynthetic and other metabolic pathways. The photosynthetic apparatus of *C. aurantiacus* exhibits an interesting combination of characteristics found in very different and diverse groups of phototrophic prokaryotes. They have a type II photoreaction center and integral membrane antenna complex reminiscent of purple bacteria (*12*, *13*). In addition, they have a peripheral chlorosome antenna complex (*14*) and a chlorophyll biosynthesis pathway that are both similar to those found in green sulfur bacteria (*15*, *16*). *C. aurantiacus* also contains a unique autotrophic carbon fixation pathway different from that found in any other phototrophs, the 3-hydroxypropinate cycle (*17*, *18*). Therefore, the phylogenetic characterization and the versatile photosynthetic apparatus of *C. aurantiacus* suggest that it occupies an important place in the origin and evolution of photosynthesis (*19*).

[†]This work was supported by Grant MCB-0646621 to R.E.B. from the Molecular Biochemistry Program of the National Science Foundation. The mass spectrometry research was supported by the National Center for Research Resources (NCRR) of the National Institutes of Health (Grant 2P41RR00954).

*To whom correspondence should be addressed: Washington University in St. Louis, One Brookings Drive, CB 1137, St. Louis, MO 63130. Telephone: (314) 935-7971. Fax: (314) 935-4432. E-mail: blankenship@wustl.edu.

 Published on Web 07/08/2010

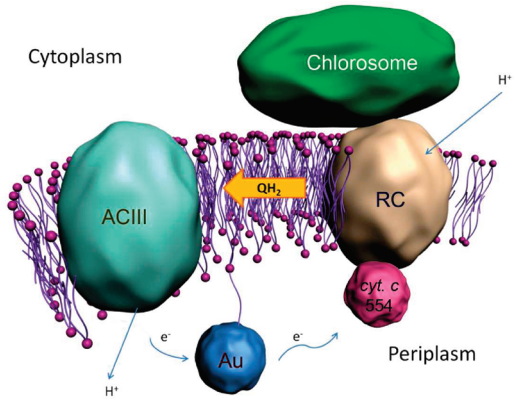

FIGURE 1: Proposed photosynthetic cyclic electron transfer pathway in *C. aurantiacus*.

An intriguing characteristic of *C. aurantiacus* is its extraordinary electron transfer pathway. For all types of photosynthetic organisms, following the initial process where the light energy transforms into chemical energy, the electrons pass through a series of electron carriers and ultimately either return to the electron donor side of the photosystem via a cyclic electron transfer pathway or reduce a terminal electron acceptor in a noncyclic electron transfer process (*1*). The overall pattern of electron transfer depends critically on the type of the organism, the environment it occupies, whether aerobic or anaerobic metabolism takes place, and what type of terminal oxidants and reductants are present. While the electron transfer pathways appear to be quite different in various groups of phototrophs, one component was until recently believed to be a constant constituent in all photosynthetic systems: the cytochrome bc_1 or b_6f complex, which transfers electrons from quinol to soluble cytochrome *c* or plastocyanin and at the same time translocates protons across the membrane, creating a transmembrane proton motive force (*20*, *21*). However, *C. aurantiacus*, like other members of the FAP phylum, does not exhibit either biochemical or genomic evidence of the existence of a related cytochrome bc_1 or b_6f complex. The lack of a cytochrome bc_1 or b_6f complex suggests that this group of organisms contains an unusual photosynthetic electron transfer pathway.

A multisubunit protein complex containing *c* type cytochromes but no characteristic features of a cytochrome bc_1 complex was isolated from *C. aurantiacus* by Yanyushin (*22*). A similar complex from *Rhodothermus marinus* is now named alternative complex III (ACIII)[1] (*23*, *24*). These two complexes have been proposed to be the functional substitute of the cytochrome bc_1 complex on the basis of gene analysis of sequenced genomes of various species (*25*) and an enzymatic study of ACIII from *R. marinus* (*23*). Recent enzyme kinetic analysis showing that ACIII performs the function of a quinol:auracyanin oxidoreductase strongly supports the hypothesis that ACIII fulfills the functional role of the cytochrome bc_1 complex in the photosynthetic electron transfer chain in *C. aurantiacus* (*26*). Figure 1 shows the proposed cyclic electron transfer pathway in *C. aurantiacus*.

On the basis of the genome arrangement of ACIII genes and early fundamental structural studies, the organization of ACIII was revealed to be entirely different from that of cytochrome bc_1 or b_6f complexes. However, a challenging question emerges: how does ACIII, a complex with structure vastly different from that of the cytochrome *bc* complex, carry out the same function in the electron transfer pathway in photosynthesis? A complete picture of the structure and role of ACIII is still missing. The key to elucidating this system is therefore believed to reside in understanding ACIII in terms of its substructure and how this relates to its function in photosynthesis and respiration. In this work, a schematic structural model of photosynthetic ACIII is proposed on the basis of chemical cross-linking of subunits in tandem with MALDI-TOF mass spectrometry. The size and type of each subunit were determined by gel electrophoresis, including one- and two-dimensional SDS−PAGE and native PAGE. The type and number of cofactors existing in ACIII were investigated using metal analysis, HPLC combined with ESI-MS, and potentiometric titrations.

MATERIALS AND METHODS

Bacterial Strains and Growth Conditions. *C. aurantiacus* strain J-10-fl was grown in batch culture anaerobically and photosynthetically in modified medium D (*13*) at 55 °C for ~72 h. Cells were harvested by centrifugation at 12000*g*, and the pellet was washed with 20 mM Tris-HCl buffer (pH 8.0) (buffer A) and then stored at −20 °C. A large-scale growth in a 16 L fermentor typically yields approximately 80 g of wet-packed cells.

Whole Membrane Isolation. *C. aurantiacus* cells were thawed and suspended in buffer A to a concentration of 1 g of wet cells per 4 mL of buffer. The cells were broken by sonication for 5 min three times in a precooled sonicator (Branson Sonifier 450) in the presence of DNase and $MgCl_2$ at 4 °C. Unbroken cells and large debris were precipitated by centrifugation at 12000*g* for 15 min. The supernatant was then ultracentrifuged at 200000*g* for 2 h. The resulting pellet, referring to whole membranes, was resuspended in buffer A to a concentration of OD = 10 at 866 nm and stored at −20 °C until further use.

Protein Purification. The whole membrane sample was thawed to room temperature and treated with reduced Triton X-100 by dropwise addition to a final concentration of 4% (w/v). Solid NaCl was added to a concentration of 0.1 M. After a 1 h incubation at room temperature with stirring, a subsequent ultracentrifugation at 200000*g* for 2 h was performed. The collected supernatant was filtered through a 0.2 μm filter and loaded onto a Q Sepharose Fast Flow 50/10 (mm/cm) column pre-equilibrated with buffer A containing 0.25% reduced Triton X-100 and 0.1 M NaCl (buffer B). The column was washed extensively with buffer B until the green color due to the solubilized free BChl *c* pigment was washed out. Afterward, the column was washed with buffer A containing a higher NaCl concentration (0.4 M) and 0.25% reduced Triton X-100. Proteins, including ACIII, ATP synthase, and menaquinone fumarate reductase (mQFR), were eluted (*27*). The eluant was diluted with buffer A to 3 three its volume and loaded onto a 75 mL Q Sepharose High Performance (QSHP) (GE Healthcare) column. Crude ACIII and other proteins, e.g., mQFR complex and ATP synthase complex, were separated with a linear gradient of NaCl from 0.1 to 0.5 M in 20 column volumes. The fractions containing crude ACIII were combined, diluted with buffer A, and loaded onto a third ion exchange

[1]Abbreviations: ACIII, alternative complex III; SDS−PAGE, sodium dodecyl sulfate−polyacrylamide gel electrophoresis; MALDI-TOF MS, matrix-assisted laser desorption ionization time-of-flight mass spectrometry; HPLC, high-performance liquid chromatography; ESI-MS, electrospray ionization mass spectrometry; DDM, dodecyl maltoside; EGS, ethylene glycol bis(succinimidylsuccinate); DSP, dithiobis(succinimidylpropionate); DSG, disuccinimidyl glutarate; NHS-ASA, *N*-hydroxysuccinimidyl-4-azidosalicylic acid; DFDNB, 1,5-difluoro-2,4-dinitrobenzene; EDC, 1-ethyl-3-[3-(dimethylamino)-propyl]carbodiimide hydrochloride; HEPES, 4-(2-hydroxyethyl)-1-piperazineethanesulfonic acid.

column, 5 mL QSHP. Afterward, further purification was performed on an S-300 (26 cm × 70 cm) gel filtration column in buffer B using concentrated crude ACIII fractions. A final purification step using a Mono Q1 column with a Bio-Rad Duo-Flow chromatography system was conducted to obtain purified ACIII for use in subsequent experiments. Detergent exchange was required for further purification. The detergent exchange process was similar to the gel filtration column purification step described above except for the change of the detergent to 0.1% dodecyl maltoside (DDM).

Electrophoresis. Tricine SDS−PAGE was performed on purified ACIII as described previously (*28*) with 12.5% T/3% C. Urea (8 M) was added to both the separating layer of the gel and the loading buffer, yielding sharp bands. Blue-Native gel electrophoresis and a following two-dimensional tricine SDS−PAGE were conducted using the method of Schägger and von Jagow (*29*). The subunit bands were tested for *c* type heme on the SDS−PAGE gel by a colorimetric heme staining assay (*30*). A series of horse heart cytochrome *c* samples of different concentrations and a purified ACIII sample were subjected to SDS−PAGE and subsequent heme staining, followed by intensity analysis using an image processing program, ImageJ (developed by the National Institutes of Health).

In-Gel Protein Digestion. Stained bands of the subunits were excised, in-gel digested with trypsin, and extracted from the gel as described previously (*31*) with modifications. The excised protein bands were destained and washed with 50% acetonitrile in 50 mM aqueous NH_4HCO_3. Proteins were then reduced with 10 mM dithiothreitol in 100 mM NH_4HCO_3 for 30 min. Cysteines in the protein peptides were further alkylated by 55 mM iodoacetamide in 100 mM NH_4HCO_3 for an additional 30 min. Trypsin (Promega Trypsin Gold, TPCK-treated) in 40 mM NH_4HCO_3 was added to the gel pieces, and the enzymatic reaction was conducted overnight at 37 °C. Afterward, peptides were extracted twice with 1% trifluoroacetic acid in 60% acetonitrile for 30 min. Extracted solutions were collected, dried completely in a speed-vac, and then redissolved in 50% acetonitrile containing 0.1% trifluoroacetic acid for analysis.

MALDI-TOF Analysis and Database Search. MALDI-TOF analyses were used to determine protein identities by peptide mass fingerprinting. Analysis was performed using an ABI 4700 MALDI-TOF mass spectrometer (Applied Biosystems). An approximately 0.5 mL mixture of the peptide sample and freshly prepared matrix solution (10 mg/mL α-cyano-4-hydroxycinnamic acid in 50% acetonitrile, 0.1% TFA aqueous solution) was spotted on a stainless steel sample plate. Each mass spectrum was the average of at least 100 laser shots and was calibrated with Data Explorer (Applied Biosystems). Peptide mass value searches were performed against the National Center for Biotechnology Information (NCBI) sequence (NCBInr) database using MASCOT Peptide Mass Fingerprint database search software (www.matrixscience.com). The alkylation of cysteine was included as a possible modification. One missed tryptic cleavage was considered, and the mass tolerance for the monoisotopic peptide masses was set to ±0.6 Da.

Metal and Cofactor Analysis. The concentration of ACIII was determined by the bicinchoninic acid protein assay (BCA assay) (Pierce). The number and type of metal atoms were determined using an AA600 atomic absorption spectrophotometer (PerkinElmer Life Sciences, Wellesley, MA). The amount of heme was quantified by pyridine hemochrome analysis using an extinction coefficient of 23.97 mM^{-1} cm^{-1} for *c* type heme (*32*). The amount of acid labile sulfur was measured by the modified methylene blue method (*33*).

Determination of the Amount of Heme by HPLC and Electrospray Ionization Mass Spectrometry (ESI-MS). The separation of heme-containing subunits in ACIII was performed on an Agilent 1100 Series HPLC system. Isolated ACIII (10 mg/mL, 10 μL) was applied at a rate of 1.0 mL/min to a C4 reverse phase HPLC column. The mobile phase consisted of water with 0.1% TFA (solvent A) and 80% acetonitrile with 20% water containing 0.09% TFA (solvent B). The following gradients were applied at a flow rate of 1.0 mL/min: linear gradient from 20 to 60% B over 30 min, linear gradient from 60 to 100% B over 50 min, 100% B for 10 min, linear gradient from 100 to 20% B over 5 min, 95 min in total, and then an isocratic elution with 20% B for at least 30 min to re-equilibrate the column for the next injection. Elution of the protein subunits was monitored at 214, 280, 415, and 525 nm. The eluant fractions were collected on the basis of the peak slope and threshold absorbance at 3 min intervals. The fractions containing targeted subunits were then concentrated to ∼20 μL by vacuum centrifugation at room temperature and injected onto a C18 guard column (1 mm × 15 mm, Optimize Technologies, Oregon City, OR). Proteins were then eluted by gradient and analyzed using a Thermo LTQ-FT mass spectrometer (Thermo Fisher, San Jose, CA).

Potentiometric Titration. Anaerobic potentiometric titrations were performed to determine the midpoint potentials (E_m) of redox-active cytochromes in ACIII. The potential was controlled using a CH 620C potentiostat (CH Instruments), and spectral changes of ACIII upon reduction and oxidation were monitored at 555 nm by a Perkin-Elmer Lambda 950 UV−vis spectrophotometer. The titration was conducted at room temperature in the presence of a mixture of the following electron mediators: methyl viologen ($E_{m,7}$ = −475 mV), benzyl viologen ($E_{m,7}$ = −357 mV), anthraquinone-2-sulfonic acid (AQS) ($E_{m,7}$ = −255 mV), anthraquinone-2,6-disulfonic acid disodium salt (AQDS) ($E_{m,7}$ = −184 mV), 2-hydroxy-1,4-naphthoquinone ($E_{m,7}$ = −145 mV), 2,5-dihydroxy-*p*-benzoquinone ($E_{m,7}$ = −60 mV), phenazine methosulfate ($E_{m,7}$ = 8 mV), phenazine ethosulfate ($E_{m,7}$ = 60 mV), Fe(III) EDTA ($E_{m,7}$ = 117 mV), 1,2-naphthoquinone-4-sulfonic acid ($E_{m,7}$ = 215 mV), 2,3,5,6-tetramethyl-*p*-phenylenediamine (DAD) ($E_{m,7}$ = 260 mV), *N*,*N*-dimethyl-1,4-phenylenediamine dihydrochloride (DMPD) ($E_{m,7}$ = 371 mV), and potassium ferricyanide ($E_{m,7}$ = 435 mV). Very concentrated ACIII was diluted into 20 mM Tris buffer (pH 7.0) to a final concentration of ∼5 mg/mL, and each mediator was added to a final concentration of 50 μM.

Low-Temperature and Room-Temperature UV−Vis Spectroscopy. UV−vis spectra of reduced and oxidized ACIII were recorded, at both room temperature and liquid nitrogen temperature, using a Perkin-Elmer Lambda 950 UV−vis spectrophotometer and a cryostat (Optistat DN, Oxford Instruments).

Transmembrane Topology Analysis and Transit Peptide Analysis. The subunits containing transmembrane helices and the transmembrane topology were predicted by hydropathy plots accessed at http://www.expasy.ch/cgi-bin/protscale.pl. The transit peptide analysis was conducted with CBS SignalP 3.0 (http://www.cbs.dtu.dk/services/SignalP/).

Chemical Cross-Linking. Chemical cross-linking was utilized to probe the subunit spatial arrangement of ACIII. The purified complex was cross-linked with EGS [ethylene glycol bis(succinimidylsuccinate)] (16.1 Å), DSP [dithiobis(succinimidylpropionate)] (12 Å), DSG (disuccinimidyl glutarate) (7.7 Å),

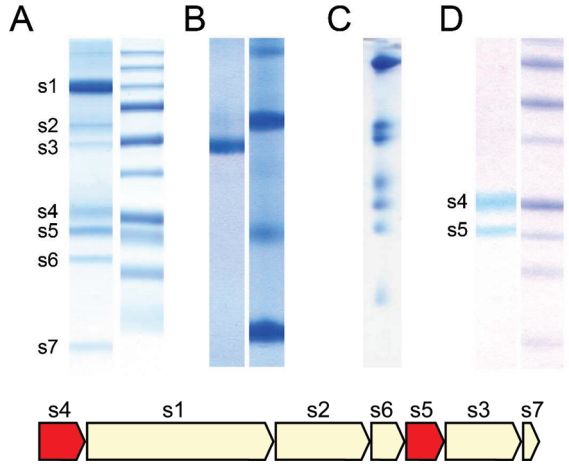

FIGURE 2: Electrophoresis analysis of isolated ACIII from *C. aurantiacus*. The graphic shown at the bottom represents the gene encoding ACIII (DOE Joint Genome Institute database). (A) Urea SDS−PAGE of purified ACIII using a 12.5% T, 3% C, and 8 M urea gel system. The right lane contained molecular mass standards (Bio-Rad), and the molecular masses of the standard proteins from bottom to top are 10, 15, 20, 25, 37, 50, 75, 100, 150, and 200 kDa. (B) Blue native PAGE of ACIII. Molecular mass standards in the right lane include BSA (66 kDa for a monomer and 132 kDa for a dimer) and ferritin (440 kDa for a monomer and 880 kDa for a dimer). (C) Two-dimensional tricine SDS−PAGE of the excised lane from the blue native gel. (D) Heme-stained tricine SDS−PAGE of purified ACIII. The right lane contained molecular mass standards (Bio-Rad), and the molecular masses of the standard proteins from bottom to top are 10, 15, 20, 25, 37, 50, and 75 kDa.

NHS-ASA (*N*-hydroxysuccinimidyl-4-azidosalicylic acid) (5.7 Å), DFDNB (1,5-difluoro-2,4-dinitrobenzene) (3.0 Å), and sulfo-NHS (*N*-hydroxysulfosuccinimide)-assisted EDC {1-ethyl-3-[3-(dimethylamino)propyl]carbodiimide hydrochloride} (0 Å) (all cross-linkers were obtained from Pierce, Rockford, IL) according to the instructions of the supplier with modifications of the reaction time or the concentration ratio between protein and cross-linker. Before cross-linking was performed, the Tris-HCl buffer (pH 8.0) used for dissolving and stabilizing ACIII was changed into 20 mM HEPES buffer (pH 7.5) using a centrifugal filter unit (Millipore). Following incubation of the protein with various cross-linkers, the reaction was quenched for 20 min with 1 M Tris-HCl (pH 7.5) to give a final concentration of 100 mM. Subsequently, SDS−PAGE was applied to the cross-linked protein (nonreducing conditions for DSP cross-linked products) and a control ACIII sample without cross-linking. The bands of potentially cross-linked subunits were then cut out of the gel and in-gel digested with trypsin as described above, and the resulting peptides were analyzed by using an ABI 4700 MALDI-TOF mass spectrometer (Applied Biosystems) and a Thermo LTQ-Orbitrap (MS/MS) mass spectrometer (Thermo Fisher).

RESULTS

Purification and Protein Chemistry of ACIII. The isolation and purification of *C. aurantiacus* ACIII were achieved by several steps of column chromatography as described in Materials and Methods. The procedure is based on a modification of the method described by Yanyushin et al. (*22*, *25*). The purified ACIII was subjected to urea SDS−PAGE, which confirmed that the protein is comprised of seven different subunits, as shown in Figure 2A. The molecular masses of the subunits range from approximately 10 to 110 kDa, consistent with the size as expected from the corresponding gene sequences of the completed *C. aurantiacus* genome. Blue native gel electrophoresis gives a single band (Figure 2B), which corresponds to a molecular mass of ca. 300 kDa, by plotting the distance of migration versus log M_r of marker proteins. This value roughly coincides with the sum of the molecular mass of each subunit (ca. 294 kDa), suggesting that ACIII is a monomer and contains at least one copy of each subunit, but it does not eliminate the possibility that ACIII may possess more than one copy of certain smaller subunits. The two-dimensional tricine SDS−PAGE of the excised lane from the blue native gel (Figure 2C) also confirmed that ACIII was comprised of seven different subunits. By heme staining the SDS−PAGE, we showed that two of the subunits contained *c* type heme, having molecular masses of ~25 and ~23 kDa (Figure 2D).

Table 1: Result of Peptide Mass Fingerprinting for the Identification of ACIII in the *C. aurantiacus* Genome

ACIII subunit	M_r[a] (kDa)	no. of fragments identified[b]	MASCOT score[b]	percent sequence coverage[b]
s1	113.0	49	124	53
s2	55.2	10	76	20
s3	45.7	7	79	25
s4	25.2	8	52	61
s5	23.0	8	61	49
s6	19.6	8	32	48
s7	12.5	9	52	58

[a]Provided by the National Center for Biotechnology Information (NCBI) database. [b]Provided by MASCOT Peptide Mass Fingerprint database search software (www.matrixscience.com).

Each subunit of ACIII observed via SDS−PAGE was excised, digested with trypsin, and analyzed by peptide fingerprinting MALDI-TOF mass spectrometry, as described in previous studies (*25*). The peptide fragment mass spectra were used for a search by the MASCOT (Matrix Science) software for protein identification, against the *C. aurantiacus* genome and the NCBI protein database. All seven subunits were conclusively identified, and the search results are summarized in Table 1. Both the MASCOT score and the percent sequence coverage indicate reliable correspondence with respect to each subunit sequence of ACIII.

UV−Vis Spectral Analysis. UV−vis absorption spectroscopy at room temperature with both reduced and oxidized ACIII was conducted, and the results are shown in Figure 3A,B. The oxidized complex exhibited amino acid absorption at 280 nm and a *c*-type cytochrome γ (Soret) band at 411 nm. Addition of dithionite resulted in reduction of the heme and gave rise to two absorption maxima at 525 nm (β band) and 555 nm (α band) and a red shift of the γ band to 418 nm. The low-temperature absorption spectra revealed more details regarding individual hemes and their different redox potentials (Figure 3D−F). When the hemes of ACIII were in their oxidized state, their UV absorbances at both room temperature and reduced temperature showed no discernible difference in the heme-characteristic wavelengths (418, 525, and 555 nm). However, in their reduced state, the environmentally different hemes could be partially resolved at low temperatures, indicating that ACIII is a multi-heme-containing protein complex. Moreover, ascorbic acid (E^0 = 58 mV) was unable to fully reduce the ACIII hemes, suggesting that some of the hemes in ACIII have midpoint potentials lower than that of ascorbic acid.

Metal and Cofactor Analysis. Determining the numbers and types of metal centers and cofactors is an essential aspect of

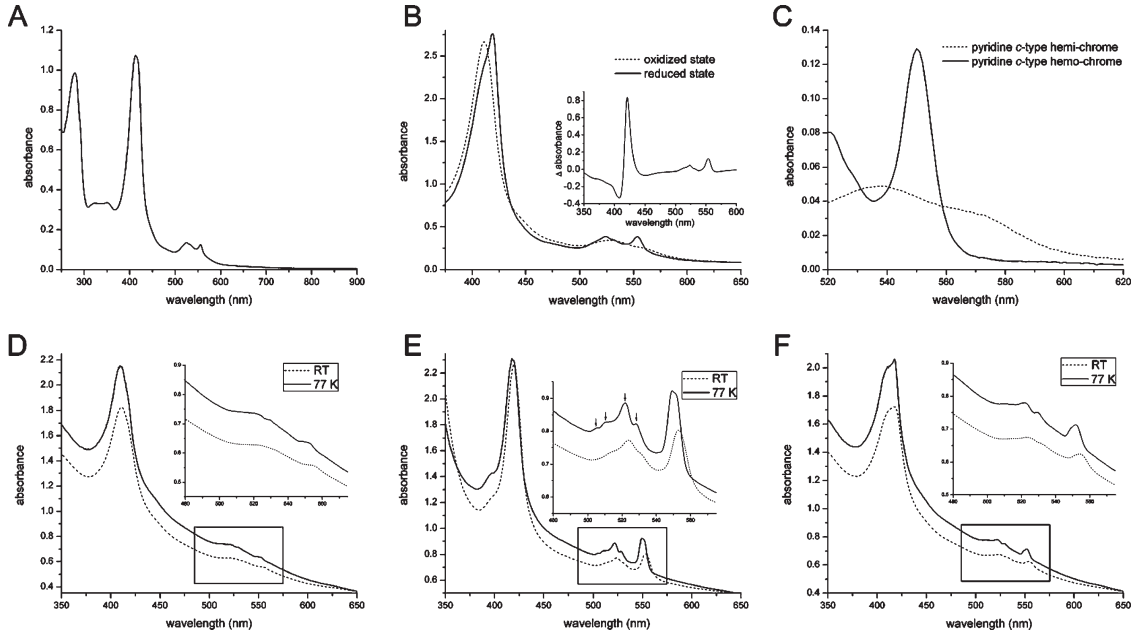

FIGURE 3: (A) UV−vis absorption spectrum of ACIII purified from *C. aurantiacus* at room temperature. (B) Spectra of the air-oxidized (---) and dithionite-reduced (—) forms from 350 to 650 nm. The inset shows the reduced-minus-oxidized difference spectrum. (C) Spectra of pyridine hemichromes *c* (---) and pyridine hemochrome *c* (—) at room temperature. (D) Spectra of air-oxidized ACIII at room temperature (---) and 77 K (—). (E) Spectra of dithionite-reduced ACIII at room temperature (---) and 77 K (—). (F) Spectra of ascorbic acid-reduced ACIII at room temperature (---) and 77 K (—).

the characterization of ACIII. Graphite furnace atomic absorption spectroscopy (AA) revealed ca. 17 (rounded from 16.9 ± 0.3) irons in one single complex and undetectable amounts of Mo and Mn. AA spectroscopy, however, does not distinguish iron in various forms, such as heme and non-heme iron. To identify the types of iron, pyridine hemochrome difference spectra (Figure 3C) were used to calculate the relative stoichiometry for *c* type hemes, the only type of heme in ACIII (*22*), which was 7 (rounded from 6.8 ± 0.1) in each complex. The remaining 10 of 17 irons were thought to be in the form of iron−sulfur clusters. To confirm this assignment, the amount of acid-labile sulfur was measured using a modified methylene blue method. It was found that there were ca. 10 (rounded from 10.3 ± 0.1) acid-labile sulfur atoms per ACIII, which gave an iron:sulfur ratio of 1:1. This value is consistent with analysis of the gene sequences of the seven ACIII subunits. Via comparison of the arrangement of cysteines in all ACIII subunits with a number of known [2Fe-2S] and [4Fe-4S] cluster-binding motifs (*34*), it was found that the largest subunit (s1) contained three apparent iron−sulfur binding motifs, while all other subunits did not contain such binding sites. Therefore, it is estimated that in ACIII, only one subunit contains iron−sulfur clusters, which are suggested to be in the form of one [2Fe-2S] cluster and two [4Fe-4S] clusters. Nevertheless, the presence of [3Fe-4S] clusters, as observed for ACIII from *R. marinus* (*23*), cannot be excluded. Future work will characterize the [Fe-S] clusters in subunit s1 using EPR spectroscopy.

Redox Potentiometry. The midpoint redox potentials of the heme cofactors of ACIII were determined using an optically transparent thin film electrode along with a potentiostat, and the data were analyzed by a method previously described (*35*). Although ACIII has more than one type of redox unit (e.g., heme and iron−sulfur cluster) functioning as electron transfer centers, in this method the *c* type hemes were selectively assayed spectrally as a function of potential. From the titration plot (Figure 4), four distinct E_m values were obtained, which were −228, −110, 94, and 391 mV versus NHE, with an intensity ratio

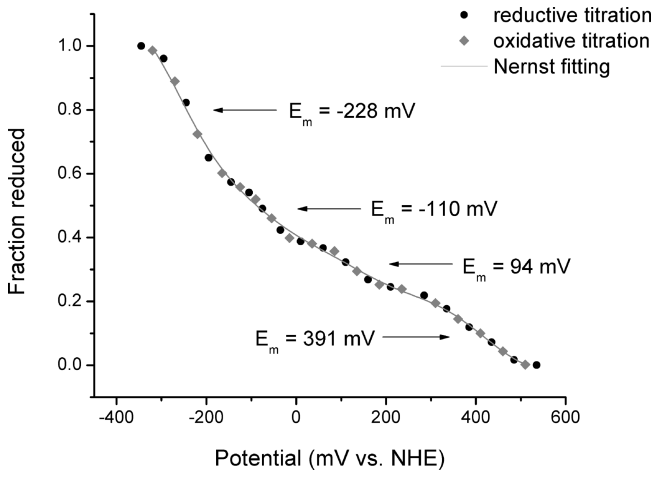

FIGURE 4: Potentiometric titration of ACIII purified from *C. aurantiacus* with squares representing the oxidative titration, black circles representing the reductive titration, and the solid line representing the Nernst fitting.

of 3:1:1:2. Assuming that the extinction coefficients are similar for all the hemes, this indicates that approximately seven hemes are present in ACIII, and that three hemes are of the lowest redox potential, two hemes are of the highest redox potential, while the other two have distinct and intermediate redox potentials. This result is consistent with the finding of seven *c* type hemes per ACIII from the pyridine hemochrome analysis. The redox titration plot also showed a reversible Nernstian behavior corresponding to one-electron oxidation−reduction reactions.

Heme Quantification by HPLC and ESI-MS. A novel approach was introduced to quantify heme in ACIII. By monitoring UV−vis absorption at 415 nm, which is characteristic of heme-containing species, we collected two fractions at 34.3 and 35.3 min from the HPLC (Figure 5A). SDS−PAGE with silver staining indicated that the two fractions corresponded with the two heme-containing subunits (s4 and s5) of ACIII (Figure 5B).

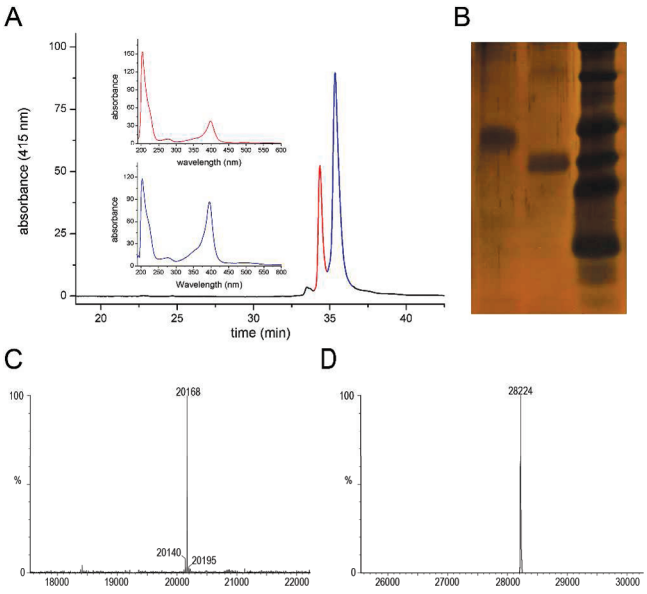

FIGURE 5: (A) Separation of the two heme-containing subunits, s4 (blue) and s5 (red), by reverse phase HPLC on a Vydac C4 column. The UV−vis absorptions of s4 and s5 are shown in the inset. (B) Analysis of the two HPLC elution peaks containing s4 (left lane) and s5 (middle lane) by silver-stained SDS−PAGE. (C) ESI mass spectrum of the ACIII s5 subunit isolated by RP-HPLC. (D) ESI mass spectrum of the ACIII s4 subunit isolated by RP-HPLC.

The peak integration ratio of the two subunits measured at 415 nm was 2:5, giving a total of seven hemes, again consistent with the number of hemes determined by pyridine hemochrome analysis and potentiometric titration. The accurate molecular masses of both of the subunits containing covalently bound heme were determined by ESI mass spectrometry to be 20168.0 (s5) and 28224.0 Da (s4), respectively (Figure 5C,D). Via comparison of the measured molecular mass against the calculated molecular mass of the peptide based on the gene sequence (s5, 19496.7 Da; s4, 25222.0 Da), which does not include the molecular mass of any cofactors, the number of hemes for each subunit was calculated by eq 1.

$$\text{number of hemes} = (\text{MW}_{\text{MS}} - \text{MW}_{\text{calc}})/\text{MW}_{\text{heme-c}} \qquad (1)$$

From the calculation, the first fraction (34.3 min), which corresponds to the smaller heme-containing subunit (s5), contained one heme (calculated value of 1.09, considering the subtraction of the predicted signal peptide). The second fraction (35.3 min) possessed five hemes (calculated value of 4.86), corresponding to the larger multi-heme-containing subunit (s4) (Figure 5A). This result is consistent with the genome analysis, which showed only one *c* type heme binding motif (CXXCH) in s5 and five *c* type heme binding sites in s4. Because the s5 subunit contains only one heme, the 2:5 ratio of the hemes of the two subunits as determined by HPLC strongly suggests that there are two copies of s5 existing in ACIII to match the stoichiometry of the hemes as determined by metal analysis, potentiometric titration, and pyridine hemochrome analysis.

Heme Quantification by Heme Staining and Intensity Analysis. The intensities of the stained bands from the two heme-containing subunits [s4 and s5 (Figure 6A)] of ACIII were quantified using ImageJ, which were then compared against a serially diluted horse heart cytochrome *c* parallel control. The intensity of the two bands from ACIII gave a ratio of ~2:5 (2.00:4.92), indicating that the numbers of hemes in the two types

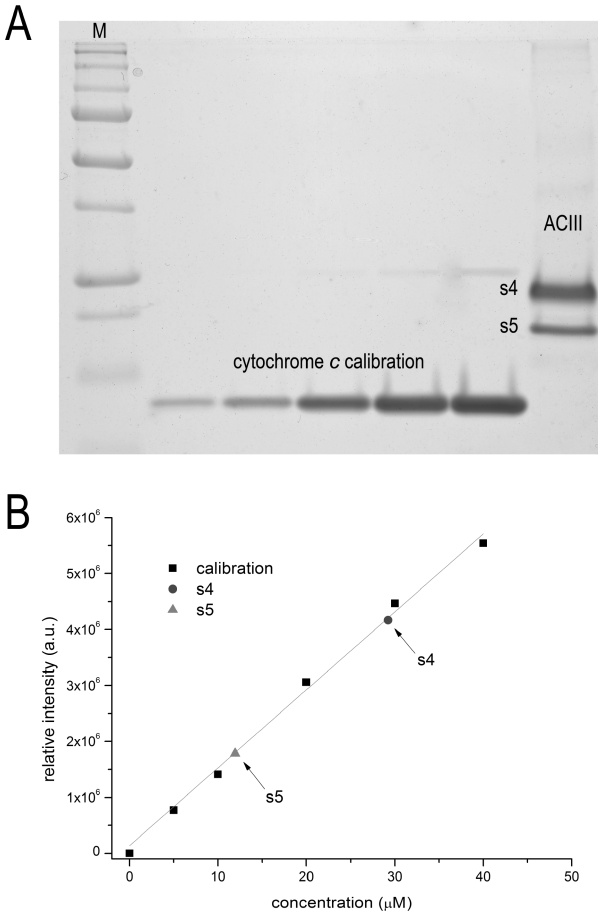

FIGURE 6: (A) Heme-stained SDS−PAGE of a series of horse heart cytochrome *c* of gradually increasing concentrations and purified ACIII (right lane). The left lane contained molecular mass standards (Bio-Rad), and the molecular masses of the standard proteins from bottom to top are 15, 20, 25, 37, 50, 75, 100, 150, and 200 kDa. (B) Calibration curve of gel band intensity vs concentration of cytochrome *c* (■) generated from panel A. The circle represents the intensity of s4 and the triangle the intensity of s5.

of subunits are two and five, respectively, assuming that the three proteins stain with equal efficiency. From Figure 6B, a calibration curve of intensity versus concentration was created from the stained bands of horse heart cytochrome *c*, to examine the concentrations of the two heme-containing subunits of ACIII. The concentration of s4 determined by the calibration curve (29.23/5 = 5.85 μM) roughly matches the concentration of ACIII determined by the BCA assay (6.12 μM), while the concentration of s5 from the calibration curve (11.88 μM) is nearly twice the concentration of ACIII (6.12 μM). These results again point toward the conclusion that ACIII contains two copies of s5 and one copy of s4.

Chemical Cross-Linking Analysis. Intracomplex cross-linking of purified ACIII was conducted with a series of bifunctional cross-linkers of various lengths (from 0 to 16 Å), including EDC/sulfo-NHS, DFDNB, NHS-ASA, DSG, DSP, and EGS. These cross-linkers are amine-reactive or can form amine-reactive intermediates and are able to react with the ε-amino group of lysine or the N-terminus of the protein. With the exception of EDC/NHS and NHS-ASA, all other cross-linkers are homobifunctional, effecting amine group couplings. EDC/NHS is a heterobifunctional, zero-length cross-linker, linking carboxylic acids and amines. NSH-ASA contains two functional ends, an amine-reactive NHS ester and a photoreactive azidosalicylic acid

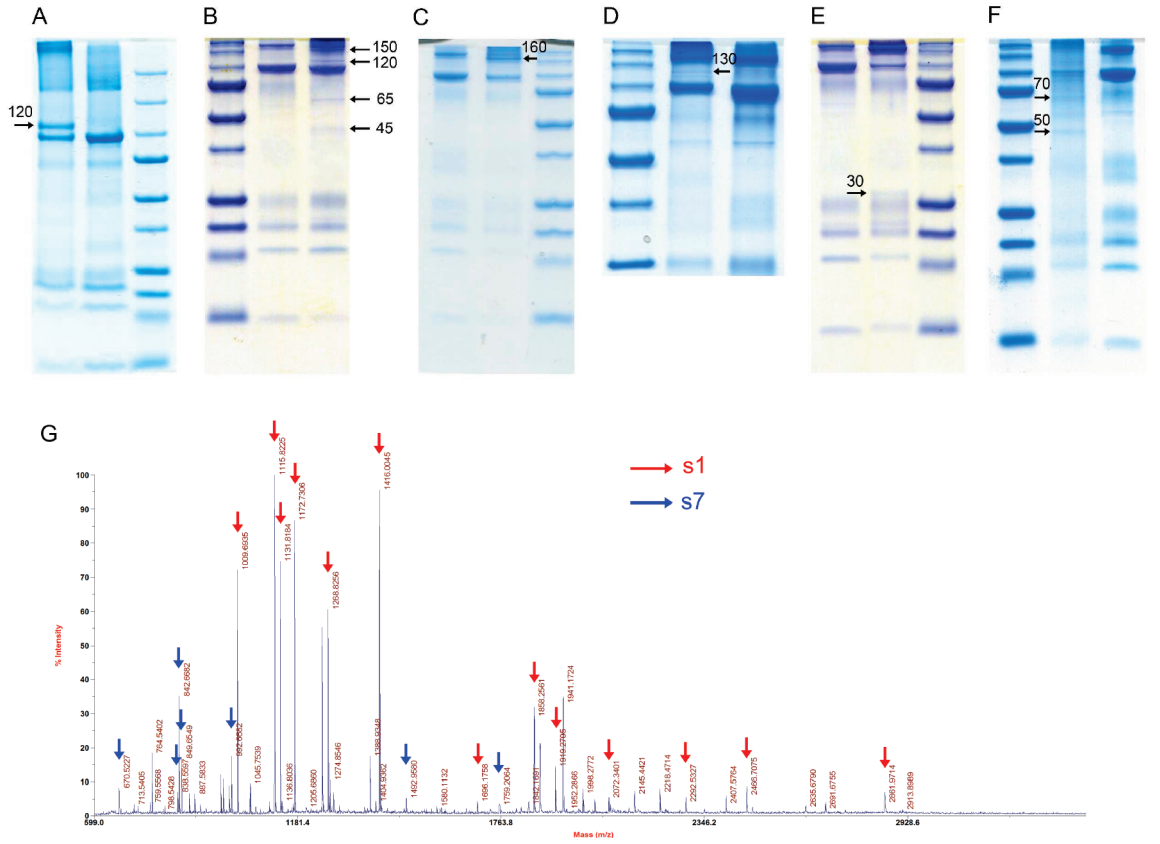

FIGURE 7: Chemical cross-linking of ACIII subunits and identification of subunit interactions. (A) Cross-linking of s1 and s7 (120 kDa) with DSP. The left lane contained cross-linked ACIII, the middle lane an ACIII control without cross-linker, and the right lane a protein standard marker (from bottom to top, 15, 20, 25, 37, 50, 75, 100, 150, and 200 kDa). (B) Cross-linking of s1, s4, and s7 (150 kDa), s1 and s7 (120 kDa), s3 and s5 (65 kDa), and two copies of s5 (40 kDa) with sulfo-NHS-assisted EDC. The right lane contained cross-linked ACIII, the middle lane an ACIII control without cross-linker, and the left lane a protein standard marker (from bottom to top, 15, 20, 25, 37, 50, 75, 100, 150, and 200 kDa). (C) Cross-linking of s1, s4, s5, and s7 (160 kDa) with EGS. The middle lane contained cross-linked ACIII, the left lane an ACIII control without cross-linker, and the right lane a protein standard marker (from bottom to top, 15, 20, 25, 37, 50, 75, 100, 150, and 200 kDa). (D) Cross-linking of s1 and s6 (125 kDa) with DFDNB. The middle lane contained cross-linked ACIII, the right lane an ACIII control without cross-linker, and the left lane a protein standard marker (from bottom to top, 25, 37, 50, 75, 100, 150, and 200 kDa). (E) Cross-linking of s4 and s7 (30 kDa) with DSG. The middle lane contained cross-linked ACIII, the left lane an ACIII control without cross-linker, and the right lane a protein standard marker (from bottom to top, 15, 20, 25, 37, 50, 75, 100, 150, and 200 kDa). (F) Cross-linking of s2 and s4 (70 kDa) and s3 and s6 (50 kDa) with NHS-ASA. The middle lane contained cross-linked ACIII, the right lane an ACIII control without cross-linker, and the left lane a protein standard marker (from bottom to top, 15, 20, 25, 37, 50, 75, 100, 150, and 200 kDa). (G) MALDI-TOF mass spectrum of cross-linked s1 and s7 using DSP. The peaks with red arrows are the characteristic peptides of s1 after trypsin digestion, and the peaks with blue arrows are the characteristic peptides of s7 after trypsin digestion.

for which the binding site is nonspecific. Intermolecular reactions were not considered competing reactions because of the relatively low concentration of the protein sample. Figure 7 displays the cross-linked products detected by SDS−PAGE with Coomassie blue staining using different cross-linkers. The cross-linking treatment gave rise to several new bands compared with the protein control. These new bands were then identified by MALDI-TOF and LC−MS/MS following trypsin digestion. The results are listed in Table 2. Cross-linking with DSP and EDC both produced the same pattern of 120 kDa products, which were then identified as cross-linked s1 and s7 (Figure 7A, B). EDC cross-linking also gave rise to two low-molecular mass products of ca. 65 and 45 kDa, and one high-molecular mass product of ~150 kDa (Figure 7B). The two low-molecular mass products were determined to be the complex of s5 and s3 and an s5 dimer. The high-molecular mass species was a trimer of s1, s7, and s4. The finding of the homodimer of s5 is convincing evidence that there are two copies of the monoheme subunit existing in ACIII. Incubation of ACIII with EGS, the longest cross-linker, produced the most complex cross-linked product, a tetramer of ~160 kDa formed by s1, s7, s4, and s5 (Figure 7C). DFDNB cross-linking gave another high-molecular mass pattern of approximately 130 kDa by linking with s1 and s6 (Figure 7D). A low-molecular mass product of around 30 kDa was observed when DSG was used, which was identified to be a dimer of s7 and s4 (Figure 7E). Cross-linking with the heterobifunctional cross-linker NHS-ASA gave two low-molecular mass bands, at ca. 70 and 50 kDa, recognized as a dimer of s2 and s4 and a dimer of s3 and s6, respectively (Figure 7F). Figure 7G shows the identification using mass spectrometry of the DSP cross-linked product as a typical example. All other spectra and identification results are included in the Supporting Information.

DISCUSSION

Instead of a cytochrome bc_1 or cytochrome b_6f complex, the phototrophic bacterium *C. aurantiacus* contains a newly discovered multisubunit integral membrane protein complex called alternative complex III. ACIII is thought to be the menaquinone:auracyanin oxidoreductase, playing a critical role in the electron transfer chain (*25*, *26*). This entirely new bioenergetic system not only provides us with an opportunity to understand *C. aurantiacus*, the earliest branching group of bacteria that have

Table 2: Identified Cross-Linked Products and Their Constituent Polypeptides[a]

cross-linker	apparent M_r of cross-linking (kDa)	subunits identified
DSP	120	s1 and s7
EDC	150	s1, s4, and s7
	120	s1 and s7
	65	s3 and s5
	45	s5 and s5
DFDNB	130	s1 and s6
DSG	30	s4 and s7
EGS	160	s1, s4, s5, and s7
NHS-ASA	70	s2 and s4
	50	s3 and s6

[a]The method is described in Materials and Methods.

the ability to perform photosynthesis (*36*), but also gives us a tool for investigating different mechanisms and evolutionary pathways involved in the electron transfer chain in various species. To improve our understanding of the intriguing role of ACIII in *C. aurantiacus*, two main problems need to be solved: the structure of the complex and the mechanism of its function in photosynthesis and respiration. We have previously investigated the function of ACIII by studying its enzymatic activities as the menaquinol:auracyanin oxidoreductase (*26*). Herein, we provide the detailed subunit and cofactor structure of the alternative complex III, which was revealed by use of various biochemical methods.

The number and size of the subunits in ACIII were determined utilizing urea SDS−PAGE, blue native gel electrophoresis in combination with two-dimensional SDS−PAGE. These experiments consistently showed seven different subunits of a wide range of molecular masses, from ca. 10 to 100 kDa, suggesting a structure of ACIII much more complicated than that of the cytochrome bc_1 or b_6f complex in other bacterial species, which usually contain three or four subunits (*20*, *37*).

Identifying the cofactors of an unknown protein is an essential aspect of protein structural and functional studies. It therefore has been one of our primary focuses in the investigation of ACIII. Among the seven subunits, s1 is the only subunit that possesses specific binding motifs for iron−sulfur clusters, while s4 and s5 contain *c* type heme-binding motifs (CXXCH), possessing five heme-binding sites and one heme-binding site, respectively. As such, the cofactors existing in ACIII should comprise both heme groups and Fe−S clusters. This hypothesis was unequivocally confirmed by atomic absorption spectroscopy, pyridine hemochrome analysis, and an acid labile sulfur assay. In addition, from low-temperature UV−vis absorption measurement, it was found that ACIII contained more than one copy of *c* type hemes. During the investigation of the number of *c* type hemes in ACIII, an apparent conflict emerged between the number of hemes determined by potentiometric titration experiments and by binding motif searching in the ACIII gene. One explanation is that there are two copies of s5 in ACIII to account for the extra heme found by potentiometric titration. This hypothesis was tested by two different experiments, one being a novel analytical method developed in our lab (HPLC in tandem with ESI-MS) and the other being the intensity analysis of heme-staining SDS−PAGE. The results of these two studies agreed very well, independently showing that there are two copies of s5 in ACIII.

ACIII from *C. aurantiacus* has many structural analogues in nonphotosynthetic species regarding subunit and cofactor composition at both the biochemical and genomic levels. For example, in *R. marinus*, an aerobic nonphototrophic Gram-negative bacterium, an atypical complex III, which is believed to be the functional equivalent of quinol:HiPIP/cytochrome *c* oxidoreductase, has been isolated and characterized (*23*, *24*, *38*, *39*). However, none of these analogues was found to possess more than one copy of their respective mono-heme-containing subunit. This unique feature of ACIII in *C. aurantiacus* may suggest a specific functional use of this extra heme-containing subunit for electron transfer in the photosynthetic electron transfer chain compared with oxidative electron transfer pathways.

Table 3: Transmembrane Helix Topology Analysis and Transit Peptide Analysis of the Subunits of ACIII from *C. aurantiacus*[a]

	s1	s2	s3	s4	s5	s6	s7
TM[b]	0	10	9	1	1	2	0
TP[c]	N	N	N	N	Y	N	N

[a]The method is described in Materials and Methods. [b]TM, transmembrane helix. [c]TP, transit peptide.

In addition to identifying the cofactors, we were also interested in understanding the spatial arrangements of the various subunits of ACIII, which may provide useful information about interpreting and understanding the connection between structure and function. To investigate the subunit topology and establish the subunit architecture of ACIII, a chemical cross-linking approach was employed. Using a series of homo- and heterobifunctional chemical cross-linkers with various spacer arm lengths, we obtained insights into the subunit arrangement of ACIII. The largest subunit (s1) was found to be in the proximity of s7, s6, and s4. Moreover, it showed no transmembrane helices (Table 3) in transmembrane topology analysis. Also lacking any transit peptide sequences, this subunit is most likely located on the cytoplasmic side of the membrane, attached to other transmembrane subunits. s7 is the only other cytoplasmic-side membrane-attached subunit of ACIII, lacking transmembrane helices and signal peptide sequences (Table 3). As a result, the cross-linking yield between s1 and s7 is significant as the specific cross-linked band (ca. 120 kDa) can be observed by using several different cross-linkers. Besides being adjacent to s1, s7 was also found to be close to s4, as evidenced by cross-linking with DSG. The second and third largest subunits (s2 and s3), which contain 10 and 9 transmembrane helices, respectively (Table 3), are the two most hydrophobic subunits, as determined from gene sequence analysis. In addition, among the seven subunits, s2 is the only subunit that was found to possess a possible quinone-binding motif, which was previously summarized by Fisher et al. (*40*). Therefore, we hypothesize that s2 is a transmembrane subunit and contains the quinone binding site. Using the chemical cross-linking approach, s2 was found to be in direct contact with s4, the multi-heme-containing subunit, indicating that the electrons of quinol may be delivered to the heme cofactors of s4 from the quinone-binding subunit, s2. The other highly hydrophobic transmembrane subunit, s3, is adjacent to s5 and s6, as detected by cross-linking with EDC and NHS-ASA, respectively. The fourth and fifth largest subunits (s4 and s5, respectively), which are found to be heme-containing subunits, are shown by genomic analysis to contain one transmembrane helix each, suggesting that they could be partially transmembrane. However, for s5, it was found that the first 20−30 amino acids starting from the N-terminus serve both as a transmembrane helix and as a transit peptide sequence, the latter of which is usually cleaved from the protein after the protein is transported to the membrane. This hypothesis was confirmed by ESI-MS of s5 separated from intact

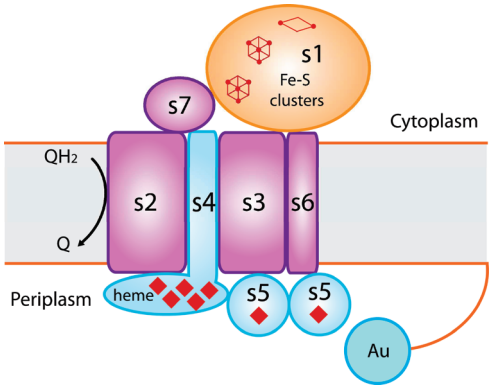

FIGURE 8: Proposed structural model of ACIII subunit architecture from *C. aurantiacus* as revealed by structural and functional studies and gene sequence analysis.

ACIII by HPLC, which shows that the mass of s5 including one heme is 20168.0 Da, 3444 Da less than the value predicted from gene sequencing (23612.0 Da). This difference in mass matches that of a transit peptide sequence. These results suggest that the two copies of s5 are transported to the outside of the membrane and attached to the periplasmic side of the membrane. This scenario was supported by the chemical cross-linking with EDC and examination with MALDI-TOF, showing a cross-linked product around twice of the molecular mass of s5 (dimeric s5). In addition, no chemical cross-linking of s5 with cytoplasm-attached subunits (s1 and s7) was found by any cross-linker used, suggesting s5 is well separated from s1 and s7, agreeing with the proposed model in which they are positioned on opposite sides of the membrane. On the basis of all the information given above, a preliminary structural model of ACIII is proposed (Figure 8).

In conclusion, in this work, as part of the effort to explore the fundamental structural characteristics of ACIII in *C. aurantiacus*, the number of hemes compared to the number of heme-binding motifs was confirmed by various biochemical methods. A structural model of ACIII interpreting the subunit−subunit interactions was proposed by utilizing chemical cross-linking and mass spectrometry. The similarity between the two ACIII forms from *C. aurantiacus* and *R. marinus* in regard to structure and function strongly suggests that ACIII from *C. aurantiacus* is another member of the alternative complex III family performing the same function as the bc_1 complex but not belonging to its family (*38*).

Many intriguing questions remain to be answered to complete the entire picture of ACIII in the electron transfer pathway. Ongoing work includes establishing the manner in which the cofactors of ACIII are tuned to transfer electrons and determining if ACIII pumps protons through the cytoplasmic membrane, which is done by the cytochrome bc_1 complex.

SUPPORTING INFORMATION AVAILABLE

Identification of the cross-linked products. This material is available free of charge via the Internet at http://pubs.acs.org.

REFERENCES

1. Blankenship, R. E. (2002) Molecular Mechanisms of Photosynthesis, Blackwell, Oxford, U.K.
2. Anraku, Y. (1988) Bacterial electron transport chains. *Annu. Rev. Biochem. 57*, 101–132.
3. Trumpower, B. L. (1990) Cytochrome bc_1 complexes of microorganisms. *Microbiol. Rev. 54*, 101–129.
4. Woese, C. R., Kandler, O., and Wheelis, M. L. (1990) Towards a natural system of organisms: Proposal for the domains Archaea, Bacteria, and Eucarya. *Proc. Natl. Acad. Sci. U.S.A. 87*, 4576–4579.
5. Blankenship, R. E. (2002) Molecular Mechanisms of Photosynthesis, Blackwell Science, Oxford, U.K.
6. Pierson, B. K., and Cashtenholz, R. W. (1995) Taxonomy and physiology of filamentous anoxygenic phototrophs. In Anoxygenic photosynthetic bacteria (Blankenship, R. E., Madigan, M. T., and Bauer, C. E., Eds.) pp 31−47, Kluwer Academic Publishers, Dordrecht, The Netherlands.
7. Pierson, B. K., and Castenholz, R. W. (1974) A phototrophic gliding filamentous bacterium of hot springs, *Chloroflexus aurantiacus*, gen. and sp. nov. *Arch. Microbiol. 100*, 5–24.
8. Keppen, O. I., Baulina, O. I., Lysenko, A. M., and Kondratieva, E. N. (1993) New green bacterium belonging to family Chloroflexaceae. *Microbiology* (*Moscow, Russ. Fed.*) *62*, 179–185.
9. Gorlenko, V. M. (1988) Ecological niches of green sulfur and gliding bacteria. In Green Photosynthetic Bacteria (Olson, J. M., Ormerod, J. G., Amesz, J., Stackebrandt, E., and Trüper, H. G., Eds.) pp 257−267, Plenum Press, New York.
10. Pierson, B. K., Giovannoni, S. J., Stahl, D. A., and Castenholz, R. W. (1985) *Heliothrix oregonensis*, gen. nov., sp. nov., a phototrophic filamentous gliding bacterium containing bacteriochlorophyll *a*. *Arch. Microbiol. 142*, 164–167.
11. Pierson, B. K., Valdez, D., Larsen, M., Morgan, E., and Mack, E. E. (1994) *Chloroflexus*-like organisms from marine and hypersaline environments: Distribution and diversity. *Photosynth. Res. 41*, 35–52.
12. Bruce, B. D., Fuller, R. C., and Blankenship, R. E. (1982) Primary photochemistry in the facultatively aerobic green photosynthetic bacterium *Chloroflexus aurantiacus*. *Proc. Natl. Acad. Sci. U.S.A. 79*, 6532–6536.
13. Pierson, B. K., and Thornber, J. P. (1983) Isolation and spectral characterization of photochemical reaction centers from the thermophilic green bacterium *Chloroflexus aurantiacus* strain J-10-fi. *Proc. Natl. Acad. Sci. U.S.A. 80*, 80–84.
14. Blankenship, R. E., and Matsuura, K. (2003) Antenna complexes from green photosynthetic bacteria. In Light-Harvesting Antenna (Green, B. R., and Parson, W. W., Eds.) pp 195−217, Kluwer, Dordrecht, The Netherlands.
15. Xiong, J., Fischer, W. M., Inoue, K., Nakahara, M., and Bauer, C. E. (2000) Molecular evidence for the early evolution of photosynthesis. *Science 289*, 1724–1730.
16. Raymond, J., Zhaxybayeva, O., Gogarten, J. P., Gerdes, S. Y., and Blankenship, R. E. (2002) Whole-genome analysis of photosynthetic prokaryotes. *Science 298*, 1616–1620.
17. Holo, H., and Sirevag, H. (1986) Autotrophic growth and CO_2 fixation of *Chloroflexus aurantiacus*. *Arch. Microbiol. 148*, 292–297.
18. Herter, S., Fuchs, G., Bacher, A., and Eisenreich, W. (2002) A bicyclic autotrophic CO_2 fixation pathway in *Chloroflexus aurantiacus*. *J. Biol. Chem. 277*, 20227–20283.
19. Blankenship, R. E. (1992) Origin and early evolution of photosynthesis. *Photosynth. Res. 33*, 91–111.
20. Berry, E. A., Guergova-Kuras, M., Huang, L.-S., and Crofts, A. R. (2000) Structure and function of cytochrome *bc* complexes. *Annu. Rev. Biochem. 69*, 1005–1075.
21. Smith, J. L., Zhang, H., Yan, J., Kurisu, G., and Cramer, W. A. (2004) Cytochrome *bc* complexes: A common core of structure and function surrounded by diversity in the outlying provinces. *Curr. Opin. Struct. Biol. 14*, 432–439.
22. Yanyushin, M. F. (2002) Fractionation of cytochromes of phototrophically grown *Chloroflexus aurantiacus*. Is there a cytochrome *bc* complex among them? *FEBS Lett. 512*, 125–128.
23. Pereira, M. M., Carita, J. N., and Teixeira, M. (1999) Membrane-bound electron transfer chain of the thermohalophilic bacterium *Rhodothermus marinus*: A novel multihemic cytochrome *bc*, a new complex III. *Biochemistry 38*, 1268–1275.
24. Pereira, M. M., Refojo, P. N., Hreggvidsson, G. O., Hjorleifsdottir, S., and Teixeira, M. (2007) The alternative complex III from *Rhodothermus marinus*: A prototype of a new family of quinol: electron acceptor oxidoreductases. *FEBS Lett. 581*, 4831–4835.
25. Yanyushin, M. F., del Rosario, M. C., Brune, D. C., and Blankenship, R. E. (2005) New class of bacterial membrane oxidoreductases. *Biochemistry 44*, 10037–10045.
26. Gao, X., Xin, Y., and Blankenship, R. E. (2009) Enzymatic activity of the alternative complex III as a menaquinol:auracyanin oxidoreductase in the electron transfer chain of *Chloroflexus aurantiacus*. *FEBS Lett. 583*, 3275–3279.
27. Xin, Y., Lu, Y.-K., Fromme, P., and Blankenship, R. E. (2009) Purification, characterization and crystallization of menaquinol:fumarate oxidoreductase from the green filamentous photosynthetic bacterium *Chloroflexus aurantiacus*. *Biochim. Biophys. Acta 1787*, 86–96.

28. Schägger, H., and von Jagow, G. (1987) Tricine-sodium dodecyl sulfate-polyacrylamide gel electrophoresis for the separation of proteins in the range of 1 to 100 kDa. *Anal. Biochem. 166*, 368–379.
29. Schägger, H., and von Jagow, G. (1991) Blue native electrophoresis for isolation of membrane protein complexes in enzymatically active form. *Anal. Biochem. 199*, 223–231.
30. Goodhew, C. F., Brown, K. R., and Pettigrew, G. W. (1984) Haem staining in gels, a useful tool in the study of bacterial c-type cytochromes. *Biochim. Biophys. Acta 852*, 288–294.
31. Henzel, W. J., Billeci, T. M., Stults, J. T., Wong, S. C., Grimley, C., and Watanabe, C. (1993) Identifying proteins from two-dimensional gels by molecular mass searching of peptide fragments in protein sequence databases. *Proc. Natl. Acad. Sci. U.S.A. 90*, 5011–5015.
32. Berry, E. A., and Trumpower, B. L. (1987) Simultaneous determination of hemes *a*, *b*, and *c* from pyridine hemochrome spectra. *Anal. Biochem. 161*, 1–15.
33. Brumby, P. E., Miller, R. W., and Massey, V. (1965) The content and possible catalytic significance of labile sulfide in some of metalloflavoproteins. *J. Biol. Chem. 240*, 2222–2228.
34. Johnson, M. K. (1994) Encyclopedia of Inorganic Chemistry, Wiley, New York.
35. Bell, P. D., Xin, Y., and Blankenship, R. E. (2009) Purification and characterization of cytochrome c_6 from *Acaryochloris marina*. *Photosynth. Res. 98*, 131–140.
36. Woese, C. R. (1987) Bacterial evolution. *Microbiol. Rev. 51*, 221–271.
37. Baniulis, D., Yamashita, E., Zhang, H., Hasan, S. S., and Cramer, W. A. (2008) Structure-function of the cytochrome b_6f complex. *Photochem. Photobiol. 84*, 1349–1358.
38. Refojo, P. N., Sousa, F. L., Teixeira, M., and Pereira, M. M. (2010) The alternative complex III: A different architecture using known building modules. *Biochim. Biophys. Acta* (in press).
39. Refojo, P. N., Teixeira, M., and Pereira, M. M. (2010) The alternative complex III of *Rhodothermus marinus* and its structural and functional association with caa_3 oxygen reductase. *Biochim. Biophys. Acta 1797*, 1477–1482.
40. Fisher, N., and Rich, P. R. (2000) A motif for quinone binding sites in respiratory and photosynthetic systems. *J. Mol. Biol. 294*, 1153–1162.